

FIG. 4.6. The GMRES convergence history for preconditioners P_1 , P_2 and P_3 in two dimensions (512^2 grid) for the bubble test problem, for GMRES restart frequency 5 (empty symbols) and 10 (filled symbols). In the left panel we set the viscosity to zero (unsteady inviscid flow) and in the right panel we set density to zero (steady viscous flow).

three dimensions, for both preconditioners P_1 and P_2 . As expected, we see most rapid convergence for $\beta = 0$, and slowest convergence for $\beta \rightarrow \infty$. For the steady state case $\theta = 0$, we do not need a pressure Poisson solve for P_2 and therefore this preconditioner is somewhat more efficient than P_1 . For intermediate β 's we get somewhat better convergence for P_1 , although the difference is small. In our experience both preconditioners show rather robust behavior for varying viscous number, viscosity and density contrast ratios, and different combinations of boundary conditions (periodic, slip, or no-slip).

cfL

4.4.3. Changing problem size. An important goal in designing solvers suitable for large-scale CFD calculations is to ensure that the total number of multigrid cycles remains essentially independent of the grid size (equivalently, grid refinement). Theoretically one expects a mild logarithmic growth for any method based on multigrid, however, in practice, this growth is barely visible for computationally-feasible system sizes. In Fig. 4.8 we show convergence histories of GMRES for varying grid sizes for the steady state bubble problem in both two and three dimensions. In the left panels we show results for P_1 and the right panels for P_2 . For this challenging variable-viscosity problem (recall that the viscosity and density contrast ratio is $r_\mu = r_\rho = 100$), P_1 shows robust convergence for all of the grid sizes tested here in both two and three dimensions, requiring no more than 200 multigrid V cycles (i.e., no more than $200/4 = 50$ GMRES iterations) to reduce the residual to essentially roundoff tolerance even for a 512^3 grid. The convergence for preconditioner P_2 shows a very mild deterioration with increasing system size, although the overall efficiency is still somewhat higher than P_1 for all system sizes tested here. Similar results were obtained using P_3 (not shown). We have confirmed that improving the subsolvers, i.e., performing more multigrid cycles per application of the preconditioners, does not aid the overall GMRES convergence, despite the substantial increase in the computational cost.

I don't see this in fig looks like P1 shows obj w sym size

It is important to point out that the exact convergence and its behavior on system size depends sensitively on the details of the multigrid algorithm (e.g., how the bottom level of the multigrid hierarchy is handled, which is typically affected by parallelization), and, most importantly, on the contrast ratio. In Fig. 4.9 we show scaling results in three dimensions for a much weaker contrast ratio $r_\mu = r_\rho = 2$. In this case we see little to no effect of the system size on the convergence rate, and the total number of GMRES iterations is less than 30.

5. Conclusions. We studied several preconditioners for solving time-dependent and steady discrete Stokes problems arising when solving fluid flow problems on a staggered finite-volume grid. All

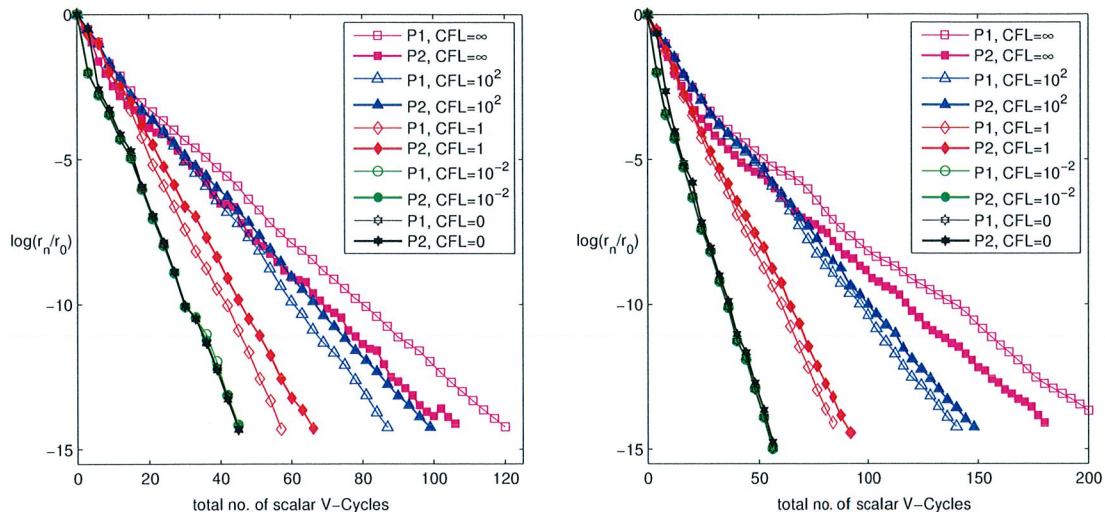


FIG. 4.7. The GMRES convergence history for preconditioners P_1 (empty symbols) and P_2 (filled symbols) in two dimensions (left panel, 512^2 grid) and in three dimensions (right panel, 128^3 grid) for the bubble test problem. We vary θ to change the viscous CFL number β from the inviscid limit $\beta = 0$ to the steady limit $\beta \rightarrow \infty$.

of these preconditioners we studied here are based on approximating the inverse of the Schur complement with a simple local operator and have been proposed before, though often limited to either constant coefficient or steady flow. By suitably approximating the inverse of the Schur complement in the case of time-dependent variable-viscosity flow we were able to easily generalize these preconditioners and thus substantially enlarge their practical applicability. We slightly modified and extended a previously proposed projection-based preconditioner P_1 to variable-coefficient flows [18]. We generalized a well-known lower triangular preconditioner P_2 to variable-coefficient flow. We extended a previously-studied “fully coupled” solver with a “local viscosity” preconditioner [16] to time-dependent flows to obtain an upper triangular preconditioner P_3 . The preconditioners investigated here can be generalized to other stable spatial discretizations of the time-dependent Stokes equations, such as finite-element schemes or adaptive mesh finite-volume discretizations.

Our primary focus was on studying the performance of these preconditioners when the pressure and velocity subsolvers are performed on a uniform staggered grid using geometric multigrid algorithms. We showed that optimal convergence rates of the GMRES Stokes solver is obtained when a single multigrid V cycle is employed as an inexact subdomain solver. We numerically observed that all three preconditioners are effective for both time-dependent and steady flow problems, with the lower and upper triangular preconditioners being more efficient for steady problems and P_1 being somewhat more efficient for time-dependent problems. All three preconditioners were found to handle variable-coefficient problems rather well, with little deterioration in convergence from the case of constant-coefficient problems. Our observations are consistent with the conclusion of the authors of Ref. [16], who “find that it is advantageous to use the FC [fully-coupled] approach utilizing relaxed tolerances for solution of the sub-problems, combined with the LV [local viscosity] preconditioner.”

All of our empirical observations are consistent with the general observation that solving the coupled Stokes problem is no more than 2-3 times more expensive than a single step of a fractional step method. We believe that this mild increase in ~~the~~ cost is more than justified given the important advantages of the the coupled approach when solving the Navier-Stokes equations. Furthermore, we observed robust behavior of the projection and lower triangular preconditioners for large systems with relatively frequent restarts. This demonstrates that GMRES with preconditioners P_1 and P_2 provides a robust solver for large-scale computations. In future studies, the robustness of these preconditioners with respect to the variability of viscosity and density should be studied more carefully. One aspect of this is whether the spectrum of the preconditioned operator can be provably bounded for

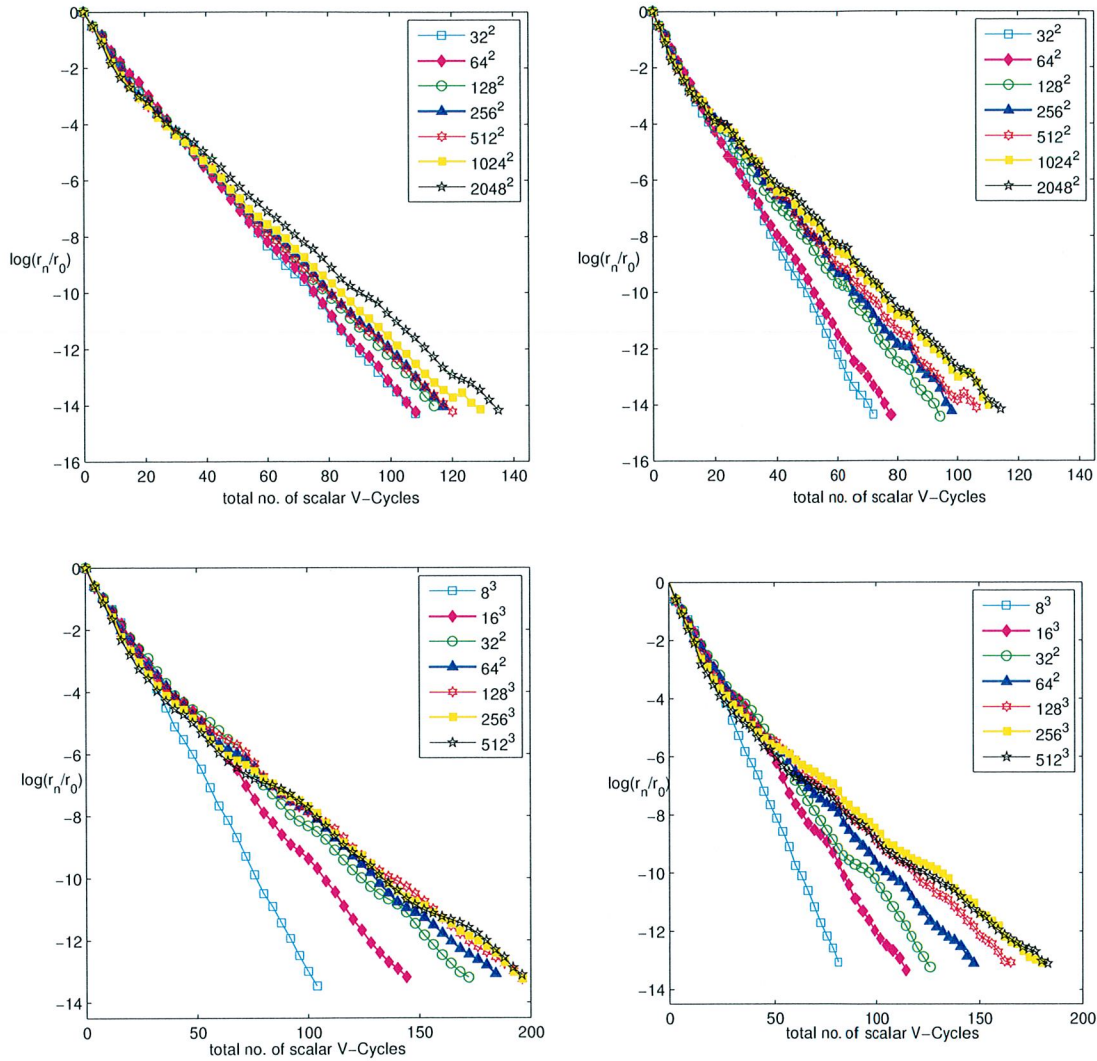


FIG. 4.8. The GMRES convergence history for preconditioners P_1 (left panels) and P_2 (right panels) in two dimensions (top panels) and in three dimensions (bottom panels) for the steady-state bubble test problem with contrast ratio $r_\mu = r_\rho = 100$, as the grid size is varied.

arbitrary contrast ratios. More importantly, however, the ~~practical~~ performance of the preconditioners in practical applications, should be accessed. Experience with steady Stokes geodynamics applications, which have extreme viscosity contrasts, are very promising [16].

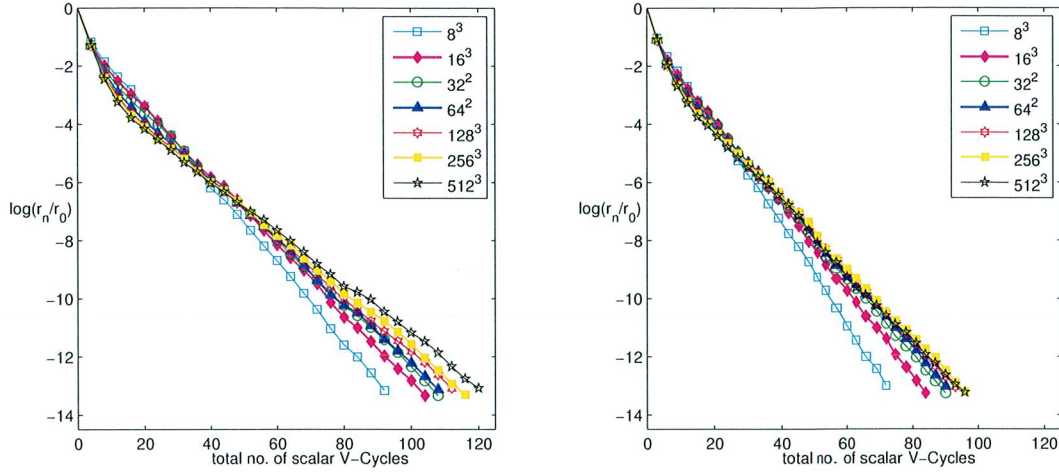


FIG. 4.9. Same as bottom two panels of Fig. 4.8 but for contrast ratio $r_\mu = r_\rho = 2$.

Appendix A. Fourier Analysis of Schur Complement.

The most important element in the preconditioners we study here is the approximation of the Schur complement inverse. In previous works, Fourier analysis [8], operator mapping properties and PDE theory in [26, 27], and commutator properties (2.4) [?, 25] have been used to justify approximations to the Schur complement inverse. Here we use Fourier analysis to justify our approximation to the Schur complement inverse for the stress form of the viscous operator (3.1). This analysis assumes periodic boundaries but should also inform the case with physical boundary conditions.

For simplicity, we use two dimensional steady state Stokes equations as illustration but extensions to three dimensions are trivial. Denote the discrete Fourier transform of velocity as $\hat{v} = [\hat{v}_x, \hat{v}_y]^T$, and denote the Fourier symbol of the staggered divergence operator as $\hat{D} = [\hat{D}_x, \hat{D}_y]$, where \hat{D}_x and \hat{D}_y represent the staggered finite difference operator along the x and y axes. The Fourier transform of the staggered gradient operator is $\hat{G} = \hat{D}^T$, and similarly, $\hat{L}_\rho = \hat{D}\hat{G} = (\hat{D}_x^2 + \hat{D}_y^2)$.

Our goal is to approximate the Schur complement inverse with a Laplacian-like local operator L_S , i.e., to find

$$(A.1) \quad (DL_\mu^{-1}G)^{-1} = L_S.$$

This is only an approximation in general but should be exact for periodic constant-coefficient problems. In Fourier space,

$$(A.2) \quad \hat{L}_S = (\hat{D}\hat{L}_\mu^{-1}\hat{G})^{-1}.$$

When the Laplacian form of the viscous term is used, $L_\mu = \mu_0 L$, we have

$$\hat{L}_\mu = \mu_0 \begin{bmatrix} \hat{D}_x^2 + \hat{D}_y^2 & 0 \\ 0 & \hat{D}_x^2 + \hat{D}_y^2 \end{bmatrix},$$

which combined with (A.2) gives $\hat{L}_S = \mu_0$. Applying an inverse Fourier transform, (A.1) becomes the well-known

$$L_S = (DL_\mu^{-1}G)^{-1} = \mu_0 I.$$

When \mathbf{L}_μ is the discrete operator for the stress tensor form of the viscous term (3.1) and the viscosity is constant, we have

$$\hat{\mathbf{L}}_\mu = \mu_0 \begin{bmatrix} 2\hat{D}_x^2 + \hat{D}_y^2 & \hat{D}_y \hat{D}_x \\ \hat{D}_x \hat{D}_y & \hat{D}_x^2 + 2\hat{D}_y^2 \end{bmatrix},$$

which gives $\hat{\mathbf{L}}_S = 2\mu_0$, and therefore $\mathbf{L}_S = 2\mu_0 \mathbf{I}$. This motivates our variable-viscosity generalization 2.6. When \mathbf{L}_μ is the discrete operator for the viscous term with bulk viscosity and assuming both the shear viscosity and the bulk viscosities are constant, we have

$$\hat{\mathbf{L}}_\mu = \begin{bmatrix} (\frac{4}{3}\mu_0 + \gamma_0)\hat{D}_x^2 + \mu_0\hat{D}_y^2 & (\frac{1}{3}\mu_0 + \gamma_0)\hat{D}_y\hat{D}_x \\ (\frac{1}{3}\mu_0 + \gamma_0)\hat{D}_x\hat{D}_y & \gamma_0\hat{D}_x^2 + (\frac{4}{3}\mu_0 + \gamma_0)\hat{D}_y^2 \end{bmatrix},$$

which gives $\hat{\mathbf{L}}_S = (\frac{4}{3}\mu_0 + \gamma_0)$ and therefore $\mathbf{L}_S = (\frac{4}{3}\mu_0 + \gamma_0) \mathbf{I}$. This motivates our variable-viscosity generalization 2.7.

Appendix B. Analysis of preconditioners with exact subsolvers.

In this Appendix we give some analysis of the spectrum of the preconditioned operators when exact pressure and velocity subsolvers are used. To see how well the different preconditioners approximate the original saddle point form (2.1), we formally calculate

$$(B.1) \quad \mathbf{P}_1^{-1} \mathbf{M} = \begin{pmatrix} \mathbf{I} & (\mathbf{I} - \rho^{-1} \mathbf{G} \mathbf{L}^{-1} \mathbf{D}) \mathbf{A}^{-1} \mathbf{G} \\ \mathbf{0} & \mathbf{S}^{-1} \mathbf{S} \end{pmatrix},$$

$$(B.2) \quad \mathbf{P}_2^{-1} \mathbf{M} = \begin{pmatrix} \mathbf{I} & \mathbf{A}^{-1} \mathbf{G} \\ \mathbf{0} & \mathbf{S}^{-1} \mathbf{S} \end{pmatrix},$$

$$(B.3) \quad \mathbf{P}_3^{-1} \mathbf{M} = \begin{pmatrix} \mathbf{I} - \mathbf{A}^{-1} \mathbf{G} \mathbf{S}^{-1} \mathbf{D} & \mathbf{A}^{-1} \mathbf{G} \\ \mathbf{S}^{-1} \mathbf{D} & \mathbf{0} \end{pmatrix},$$

and lastly

$$(B.4) \quad \mathbf{P}_4^{-1} \mathbf{M} = \begin{pmatrix} \mathbf{I} & \mathbf{A}^{-1} \mathbf{G} \\ \mathbf{S}^{-1} \mathbf{D} & \mathbf{0} \end{pmatrix}.$$

Recall that for constant-coefficient problems with exact subsolvers, $\mathbf{S}^{-1} = -\theta \rho_0 \mathbf{L}_p^{-1} + \mu_0 \mathbf{I}$. For periodic domains, the finite-difference operators \mathbf{G} , \mathbf{D} , \mathbf{L} and \mathbf{L}_p commute,

$$(B.5) \quad \mathbf{G} \mathbf{L}_p = \mathbf{L} \mathbf{G} \quad \text{and} \quad \mathbf{L}_p \mathbf{D} = \mathbf{D} \mathbf{L},$$

and therefore $\mathbf{P}_1^{-1} \mathbf{M}$ is exactly the discrete identity operator, and similarly, the (1,1) diagonal block of $\mathbf{P}_3^{-1} \mathbf{M}$ is zero.

From (B.1), we see that the preconditioned system is block upper triangular. Therefore,

$$(B.6) \quad \det(\lambda \mathbf{I} - \mathbf{P}_1^{-1} \mathbf{M}) = \det((\lambda - 1) \mathbf{I}) \det(\lambda \mathbf{I} - \mathbf{S}^{-1} \mathbf{S}),$$

which shows that the eigenvalues of the preconditioned system are either unity or the eigenvalues of $\mathbf{S}^{-1} \mathbf{S}$. Similarly, we can derive the eigenvalues of the preconditioned system using (B.2) and (B.3). Alternatively, one can write down the generalized eigenvalue system, for instance,

$$\mathbf{M} \begin{pmatrix} \mathbf{u} \\ p \end{pmatrix} = \lambda \mathbf{P}_3 \begin{pmatrix} \mathbf{u} \\ p \end{pmatrix}$$

Again, one can see that the eigenvalues are either 1 or the eigenvalues of $\mathbf{S}^{-1} \mathbf{S}$.

When $\mu_0 = 0$, or equivalently, $\Delta t \rightarrow 0$, we get the inviscid operator

$$\mathbf{M} = \begin{pmatrix} \frac{\rho_0}{\Delta t} \mathbf{I} & \mathbf{G} \\ -\mathbf{D} & \mathbf{0} \end{pmatrix},$$

and therefore $\mathbf{P}_1^{-1} \mathbf{M} = \mathbf{I}$, regardless of the boundary conditions. If \mathbf{P}_2 is used, we have

$$(B.7) \quad \mathbf{P}_2^{-1} \mathbf{M} = \begin{pmatrix} \mathbf{I} & \frac{\Delta t}{\rho_0} \mathbf{G} \\ \mathbf{0} & \mathbf{I} \end{pmatrix},$$

and therefore $(\mathbf{P}_2^{-1} \mathbf{M} - \mathbf{I})^2 = \mathbf{0}$. This proves that in the inviscid case, the GMRES algorithm converges in 1 iteration when preconditioner \mathbf{P}_1 is used, and in 2 iterations when \mathbf{P}_2 or \mathbf{P}_3 are used. When inexact subsolvers are used our numerical results showed that all three preconditioners exhibit exactly the same convergence rate in the inviscid case.

Furthermore, for constant viscosity ($\mu = 1$) steady state ($\theta = 0$) problems on a two-dimensional domain of $n_x \times n_y$ grid cells with no-slip boundaries, one can prove the following property for the eigenvalues of the Schur complement $\mathbf{S} = \mathbf{D} \mathbf{L}^{-1} \mathbf{G}$:

1. $\lambda(\mathbf{S}) \in \{0\} \cup [\eta^2, 1]$, where η is the inf-sup constant independent of grid size [15, 31].
2. The multiplicity of the 0 eigenvalue is 1.
3. There are at most $2(n_x - 1) + 2(n_y - 1)$ non-unit eigenvalues¹ of \mathbf{S} .

This is a quantitative statement of the intuitive expectation that a few cells away from the boundaries \mathbf{S} is close to an identity operator, just as for a periodic system (see Eq. (B.5)). The proof of these statements will be given in future publications, and extensions to variable-coefficient problems will be considered [21, 20]. The lower bound of the eigenvalues is a consequence of the uniform div-stability [14, 15, 41]. From (B.1) and (B.6) (and also (B.2) and (B.3)), we see that the same conclusions hold for the preconditioned systems. This analysis explains the good performance of the simple Schur complement approximation even in the presence of nontrivial boundary conditions [18].

Appendix C. Multigrid algorithms.

We employ a standard V-cycle multigrid approach [6] for both the cell-centered multigrid subsolver for the weighted Poisson operator \mathbf{L}_ρ and the staggered velocity multigrid subsolver for the viscous operator \mathbf{L}_μ . We use the standard residual formulation, so that on all coarsened levels we are solving for the error in the coarsened residual from the next-finer level. In our implementation, the multigrid coarsening factor is 2, and coarsening continues until the coarsest grid contains two grid points (with respect to cell-centers) in any given spatial direction (for parallel computations, this applies to the subgrid owned by each of the processors). At the coarsest level of the multigrid hierarchy, we perform a large (8 or more) number of relaxations, to ensure that the preconditioner is a constant linear operator. Alternatively, one can use an exact (to within roundoff) coarse solver (e.g., another iterative solver with tight tolerance or a serialized direct sparse solver).

Multigrid consists of 3 major components: (i) choice of relaxation at a particular level, (ii) coarsening/restriction operator, and (iii) interpolation/prolongation operator.

Relaxation. Both the staggered and cell-centered solvers use multicolored Gauss-Seidel smoothing. The cell-centered solver uses standard red-black relaxation, whereas the staggered solver uses a $2d$ -colored relaxation, where d is the dimensionality of the problem. Because the coupling between the DOFs corresponding to a given component of velocity is the same as for the cell-centered Poisson equation, by coloring each component of the velocity separately, as in the standard red-black coloring (i.e., coloring odd grid points with a different color from the even grid points), we obtain decoupling between the $2d$ colors so that each color can be relaxed separately (improving convergence and aiding parallelization). We relax the components of velocity in turn (i.e., in three dimensions, we order the relaxations as red-x, black-x, red-y, black-y, red-z, black-z), although other orderings of the colors are possible. Refer to Figure C.1 for a physical representation of the viscous operator stencils.

¹For boundary condition with x -direction periodic and y -direction Dirichlet [32], there are at most $2n_x$ non-unit eigenvalues of \mathbf{S} .

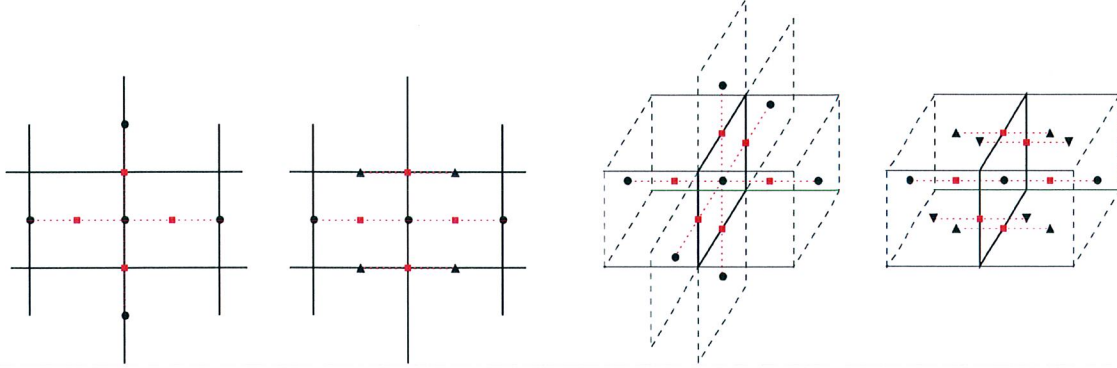


FIG. C.1. (Left panel) The stencils for the x-component of $\nabla \cdot \beta \nabla \phi$ (left) and $\nabla \cdot \beta (\nabla \phi)^T$ (right). The black circles indicate locations of u . The black triangles indicate locations of v . The red dots indicate the location of the β and the gradients of velocity. (Right panel) The stencils for the x-component of $\nabla \cdot \beta \nabla \phi$ (left) and $\nabla \cdot \beta (\nabla \phi)^T$ (right). The black circles indicate locations of u . The black triangles indicate locations of v and w . The red dots indicate the location of the β and the gradients of velocity.

Given a cell-centered operator of the form, $\nabla \cdot \beta \nabla \phi \equiv \mathcal{L}\phi = r$, or a staggered operator of the form, $\alpha\phi - \nabla \cdot \beta [\nabla \phi + (\nabla \phi)^T] \equiv \mathcal{L}\phi = r$, the relaxation takes the form

$$(C.1) \quad \phi^{k+1} = \phi^k + \omega \mathcal{D}^{-1} (r - \mathcal{L}\phi^k)$$

for each color in turn, where the superscript represents the iterate, and \mathcal{D}^{-1} is the inverse of the diagonal elements of \mathcal{L} . We use unit weighting factor², $\omega = 1$ (suggested to be near-optimal in numerical experiments) for both subsolvers.

Restriction. For the cell-centered solver, restriction is a simple averaging of the 2^d fine cells. For the staggered solver, we use a slightly more complicated 6-point ($d = 2$) or 12-point ($d = 3$) stencil. For example, for x-faces we use [Donev: I have not checked these, Andy, please double check]

$$(C.2) \quad \phi_{i,j}^c = \frac{1}{8} (\phi_{2i-1,2j}^f + \phi_{2i-1,2j+1}^f + \phi_{2i+1,2j}^f + \phi_{2i+1,2j+1}^f) + \frac{1}{4} (\phi_{2i,2j}^f + \phi_{2i,2j+1}^f)$$

As seen in Figure C.1, for the staggered solver we require α at faces, and β at both cell-centers and nodes ($d = 2$) or edges ($d = 3$). When creating coefficients at coarser levels, we obtain α by averaging the overlaying fine faces, cell-centered β by averaging the overlaying fine cell-centered values, β on nodes through direct injection, and β on edges by averaging the overlaying fine edges.

Prolongation. For the cell-centered solver, prolongation is simply direct injection from the coarse cell to the overlaying 2^d fine cells. For the staggered solver, we use a slightly more complicated stencil that involves linear interpolation for fine faces that overlay coarse faces, and bilinear interpolation for fine faces that do not overlay coarse faces. For example, for x-faces we use

$$(C.3) \quad \phi_{i,j}^f = \frac{3}{4} \phi_{i/2,j/2}^c + \frac{1}{4} \phi_{i/2,j/2-1}^c, \quad \text{for } i \text{ and } j \text{ both even,}$$

$$(C.4) \quad \phi_{i,j}^f = \frac{3}{8} (\phi_{i/2,j/2}^c + \phi_{i/2+1,j/2}^c) + \frac{1}{8} (\phi_{i/2,j/2-1}^c + \phi_{i/2+1,j/2-1}^c), \quad \text{for } i \text{ odd and } j \text{ even,}$$

where we use integer division in the index subscripts.

REFERENCES

²Note that for Jacobi relaxation with the stress form of the viscous operator, a standard analysis suggests $\omega = 1/2$ as the optimal relaxation parameter (ensuring damping of all modes).

- [1] A. ALMGREN, J. BELL, AND W. CRUTCHFIELD, *Approximate projection methods: Part I. Inviscid analysis*, SIAM Journal on Scientific Computing, 22 (2000), p. 1139. 1
- [2] A. S. ALMGREN, J. B. BELL, P. COLELLA, L. H. HOWELL, AND M. L. WELCOME, *A conservative adaptive projection method for the variable density incompressible Navier-Stokes equations*, J. Comput. Phys., 142 (1998), pp. 1–46. 1, 1, 1, 2, 3.2
- [3] J. B. BELL, P. COLELLA, AND H. M. GLAZ, *A second order projection method for the incompressible Navier-Stokes equations*, J. Comp. Phys., 85 (1989), pp. 257–283. 1, 1, 2.1
- [4] M. BENZI, *Preconditioning techniques for large linear systems: a survey*, Journal of Computational Physics, 182 (2002), pp. 418–477. 1
- [5] M. BENZI, G. H. GOLUB, AND J. LIESEN, *Numerical solution of saddle point problems*, Acta numerica, 14 (2005), pp. 1–137. 1
- [6] W. L. BRIGGS, V. HENSON, AND S. MCCORMICK, *A multigrid tutorial society for industrial and applied mathematics*, Philadelphia, PA, (1987). 4, C
- [7] D. L. BROWN, R. CORTEZ, AND M. L. MINION, *Accurate projection methods for the incompressible Navier-Stokes equations*, Journal of Computational Physics, 168 (2001), pp. 464–499. 1, 2
- [8] J. CAHOUE ET AL. AND J.-P. CHABARD, *Some fast 3d finite element solvers for the generalized stokes problem*, International Journal for Numerical Methods in Fluids, 8 (1988), pp. 869–895. 2.2, 2.3, 2.4, A
- [9] A. J. CHORIN, *Numerical Solution of the Navier-Stokes Equations*, J. Math. Comp., 22 (1968), pp. 745–762. 1, 2.1
- [10] A. DONEV, A. J. NONAKA, Y. SUN, T. G. FAI, A. L. GARCIA, AND J. B. BELL, *Low Mach Number Fluctuating Hydrodynamics of Diffusively Mixing Fluids*. Submitted to SIAM J. Multiscale Modeling and Simulation, 2013. 1, 3, 3.1
- [11] W. E AND J. LIU, *Gauge method for viscous incompressible flows*, Commun. Math. Sci., 1 (2003), pp. 317–332. 1
- [12] M. EIERMANN AND O. G. ERNST, *Geometric aspects of the theory of krylov subspace methods*, Acta Numerica, 10 (2001), pp. 251–312. 4.3.1
- [13] H. ELMAN, V. E. HOWLE, J. SHADID, R. SHUTTLEWORTH, AND R. TUMINARO, *A taxonomy and comparison of parallel block multi-level preconditioners for the incompressible navier-stokes equations*, Journal of Computational Physics, 227 (2008), pp. 1790–1808. 1
- [14] H. C. ELMAN, *Preconditioning for the steady-state navier-stokes equations with low viscosity*, SIAM Journal on Scientific Computing, 20 (1999), pp. 1299–1316. 1, 2, 2, B
- [15] H. C. ELMAN, D. J. SILVESTER, AND A. J. WATHEN, *Finite Elements and Fast Iterative Solvers: with Applications in Incompressible Fluid Dynamics: with Applications in Incompressible Fluid Dynamics*, OUP Oxford, 2005. 1, 1, 1, 2.4, 1, B
- [16] M. FURUICHI, D. A. MAY, AND P. J. TACKLEY, *Development of a stokes flow solver robust to large viscosity jumps using a schur complement approach with mixed precision arithmetic*, Journal of Computational Physics, 230 (2011), pp. 8835–8851. 1, 1, 2, 2, 2.3, 3.2, 4.2.2, 5
- [17] T. V. GERYA, D. A. MAY, AND T. DURETZ, *An adaptive staggered grid finite difference method for modeling geodynamic Stokes flows with strongly variable viscosity*, Geochemistry, Geophysics, Geosystems, 14 (2013), pp. 1200–1225. 1, 1, 1
- [18] B. GRIFFITH, *An accurate and efficient method for the incompressible Navier-Stokes equations using the projection method as a preconditioner*, J. Comp. Phys., 228 (2009), pp. 7565–7595. 1, 1, 1, 2, 2, 2.1, 2.1, 5, B
- [19] ———, *Immersed boundary model of aortic heart valve dynamics with physiological driving and loading conditions*, Int J Numer Meth Biomed Eng. 28 (2012), pp. 317–345. 1, 1
- [20] P. GRINEVICH, *An iterative solution method for the stokes problem with variable viscosity*, Moscow University Mathematics Bulletin. 65 (2010), pp. 119–122. 4.1, B
- [21] P. GRINEVICH AND M. OLSHANSKII, *An iterative method for the stokes-type problem with variable viscosity*, SIAM Journal on Scientific Computing, 31 (2009), pp. 3959–3978. 4.1, B
- [22] J. GUERMOND, P. MINEV, AND J. SHEN, *An overview of projection methods for incompressible flows*, Computer Methods in Applied Mechanics and Engineering, 195 (2006), pp. 6011–6045. 3.1
- [23] F. HARLOW AND J. WELCH, *Numerical calculation of time-dependent viscous incompressible flow of fluids with free surfaces*, Physics of Fluids, 8 (1965), pp. 2182–2189. 1, 3.1
- [24] I. C. IPSEN, *A note on preconditioning nonsymmetric matrices*, SIAM Journal on Scientific Computing, 23 (2001), pp. 1050–1051. 1, 2.2, 2.3, 4.3.1
- [25] D. KAY, D. LOGHIN, AND A. WATHEN, *A preconditioner for the steady-state navier-stokes equations*, SIAM Journal on Scientific Computing, 24 (2002), pp. 237–256. 1, 2.2, 2.3, 2.4, A
- [26] K.-A. MARDAL AND R. WINTHER, *Uniform preconditioners for the time dependent stokes problem*, Numerische Mathematik, 98 (2004), pp. 305–327. 1, 2.2, 2.3, 2.4, A
- [27] ———, *Preconditioning discretizations of systems of partial differential equations*, Numerical Linear Algebra with Applications. 18 (2011), pp. 1–40. 1, 2.2, 2.3, 2.4, A
- [28] M. F. MURPHY, G. H. GOLUB, AND A. J. WATHEN, *A note on preconditioning for indefinite linear systems*, SIAM Journal on Scientific Computing, 21 (2000), pp. 1969–1972. 1, 4.3.1
- [29] M. OLSHANSKII, *Multigrid analysis for the time dependent stokes problem*, Mathematics of Computation, 81 (2012), pp. 57–79. 1
- [30] M. A. OLSHANSKII, J. PETERS, AND A. REUSKEN, *Uniform preconditioners for a parameter dependent saddle point problem with application to generalized stokes interface equations*, Numerische Mathematik, 105 (2006), pp. 159–191. 1, 1
- [31] M. A. OLSHANSKII AND E. V. CHIZHONKOV, *On the best constant in the inf-sup-condition for elongated rect-*

- angular domains*, Mathematical Notes, 67 (2000), pp. 325–332. 1, 3.1, 1
- [32] S. ORSZAG, M. ISRAELI, AND M. DEVILLE, *Boundary conditions for incompressible flows*, Journal of Scientific Computing, 1 (1986), pp. 75–111. 1
- [33] R. PEMBER, L. HOWELL, J. BELL, P. COLELLA, W. CRUTCHFIELD, W. FIVELAND, AND J. JESSEE, *An adaptive projection method for unsteady, low-Mach number combustion*, Combustion Science and Technology, 140 (1998), pp. 123–168. 1, 1
- [34] C. RENDLEMAN, V. BECKNER, M. LIJEWSKI, W. CRUTCHFIELD, AND J. BELL, *Parallelization of structured, hierarchical adaptive mesh refinement algorithms*, Computing and Visualization in Science, 3 (2000), pp. 147–157. Software available at <https://ccse.lbl.gov/BoxLib>. 3.2
- [35] T. RUSTEN AND R. WINTHER, *A preconditioned iterative method for saddlepoint problems*, SIAM Journal on Matrix Analysis and Applications, 13 (1992), pp. 887–904. 3.2
- [36] Y. SAAD, *A flexible inner-outer preconditioned gmres algorithm*, SIAM Journal on Scientific Computing, 14 (1993), pp. 461–469. 4
- [37] Y. SAAD AND M. H. SCHULTZ, *Gmres: A generalized minimal residual algorithm for solving nonsymmetric linear systems*, SIAM Journal on scientific and statistical computing, 7 (1986), pp. 856–869. 4
- [38] D. SHIN AND J. C. STRIKWERDA, *Inf-sup conditions for finite-difference approximations of the Stokes equations*, Journal of the Australian Mathematical Society-Series B, 39 (1997), pp. 121–134. 1, 3.1
- [39] S. TUREK, *Efficient Solvers for Incompressible Flow Problems: An Algorithmic and Computational Approach*, vol. 6, Springer Verlag, 1999. 1, 1
- [40] F. B. USABIAGA, J. B. BELL, R. DELGADO-BUSCALIONI, A. DONEV, T. G. FAI, B. E. GRIFFITH, AND C. S. PESKIN, *Staggered Schemes for Incompressible Fluctuating Hydrodynamics*, SIAM J. Multiscale Modeling and Simulation, 10 (2012), pp. 1369–1408. 3, 3.1, 3.1
- [41] R. VERFÜRTH, *A multilevel algorithm for mixed problems*, SIAM journal on numerical analysis, 21 (1984), pp. 264–271. B